Polyhedron 100 (2015) 121–131

Contents lists available at ScienceDirect

Polyhedron

journal homepage: www.elsevier.com/locate/poly

Synthesis, characterization and antimicrobial activity of new Cu(II) and Zn(II) complexes with Schiff bases derived from trimethylsilyl-propyl-*p*-aminobenzoate

Mirela-Fernanda Zaltariov [a], Maria Cazacu [a,*], Mihaela Avadanei [a], Sergiu Shova [a], Mihaela Balan [a], Nicoleta Vornicu [b], Angelica Vlad [a], Anatolie Dobrov [c], Cristian-Dragos Varganici [a]

[a] "Petru Poni" Institute of Macromolecular Chemistry, Aleea Gr. Ghica Voda 41 A, Iasi 700487, Romania
[b] Metropolitan Center of Research T.A.B.O.R, The Metropolitanate of Moldavia and Bukovina, Iasi, Romania
[c] Institute of Inorganic Chemistry of the University of Vienna, Währinger Strasse 42, A-1090 Vienna, Austria

ARTICLE INFO

Article history:
Received 11 May 2015
Accepted 10 July 2015
Available online 18 July 2015

Keywords:
Mononuclear complexes
Schiff bases
Silicon derivative
Photophysical properties
Biological activity

ABSTRACT

Three mononuclear complexes, one of Cu(II) {**[Cu(L^A)$_2$]** (**4**)}, and two of Zn(II) {**[Zn(L^A)$_2$]** (**5**) and **[Zn(L^B)$_2$(H$_2$O)$_2$]$^{2+}$** (**6**)} have been synthesized through treating the corresponding metal salts with Schiff bases of trimethylsilyl-propyl-*p*-aminobenzoate with salicylaldehyde **HL^A (2)** and *o*-vanillin **HL^B (3)**. The Schiff base ligands and their metal complexes were structurally confirmed by spectral techniques (FTIR, ^{1}H NMR, ^{13}C NMR, ESI-MS, elemental analysis) and single crystal X-ray diffraction. Crystallographic data revealed different coordination environments of the metal ions: a strict square-planar geometry of the copper ion in **4**, a distorted tetrahedral geometry of the zinc ion in **5**, and an usual (O_6) octahedral coordination of the zinc ion in **6**. Spectral analysis of optical emission indicated that Zn(II) complexes exhibit strong fluorescence properties as compared with the ligands and Cu(II) complex. Thermogravimetric analysis results suggested a lower stability of the metal complexes in comparison with the free ligands. The antifungal and antibacterial properties of the prepared compounds against *Aspergillus fumigatus* ATCC 66567, *Penicillium chrysogenum* ATCC 20044, *Fusarium* ATCC 20327, *Bacillus sp.* ATCC 31073, *Pseudomonas sp.* ATCC 15780 were evaluated. Both Schiff bases and metal complexes showed better antimicrobial activity compared to the standard compounds Caspofungin and Kanamycin.

1. Introduction

Organosilicon compounds have proved particularly interest since many years ago due to their attractive properties: moisture and air stability, low toxicity, good biocompatibility and solubility [1,2]. The essential characteristics of the silicon atom (higher volume, more electropositive than carbon, the presence of *d* orbitals) determine its different chemical behavior as compared to carbon atom, which is in the same group. It can form four covalent bonds, but the presence of accessible *d* orbitals allows the formation of compounds with a higher coordination number. This ability of Si atom to expand its valence state has been extensively applied in organometallic and coordination chemistry [3]. The wide interest in organosilicon compounds is also due to their biological importance, such as anti-tumor and protease inhibition. In addition, these compounds can be used as silylating agents in various syntheses to protect certain functional groups (the dehydrogenative coupling of a silane with an alcohol) or can improve the reactivity and selectivity of the chemical species with active hydrogen (alcohols, acids, amines) [4,5]. Rapid development of organometallic chemistry, in the early 1950s, resulted in the emergence of a remarkable variety of molecular structures and of new active compounds in catalysis. A special attention was paid to the silyl-ferrocene derivatives, which showed an improved solubility in nonpolar solvents due to the presence of the silyl groups and interesting physico–chemical and redox properties [6,7]. On the other hand, organosilicon derivatives are known for their ability to function as ligands in coordination chemistry through silicon atom [8–11]. From this perspective, bimetallic or heterobimetallic silyl complexes were noted for their special structural properties as a result of the affinity of ligands for metal ions. Such compounds combine the properties of both metal–metal and metal–ligand bonds [12,13]. On the other hand, the chemistry of silicon-based ligands with different donor atoms (N, O or S) in the structure has been effectively developed in the last period, varying the range

* Corresponding author. Tel.: +40 232 217454, fax: +40 232 211299.
E-mail address: mcazacu@icmpp.ro (M. Cazacu).

http://dx.doi.org/10.1016/j.poly.2015.07.030
0277-5387/

and the coordination mode of transition metals to these ligands. The presence of the silyl moieties in the structure will provide flexibility, hydrophobicity and improved solubility in organic solvents [14–19]. The design of such structures with specific functionalities and properties is an accessible way to diversify the range of ligands, which are involved in coordination of metal ions.

From these aspects, we intend to obtain new metal complexes derived from silicon-containing Schiff bases. In the last years, metal complexes of various Schiff bases which may act as bidentate (NO), tridentate (N_2O, NO_2) or tetradentate (N_2O_2) ligands have been intensively investigated due to their interesting structural diversity as well as their analytical, biological and industrial applications. A large number of these compounds have proven antitumor, antibacterial, antifungal, antiviral properties [20–22]. The design of the Schiff base ligands begins with a rational choice of carbonylic and aminic precursors. Salicylaldehyde and its different substituted derivatives are the most widely used carbonylic compounds to obtain such ligands. Beside them, aliphatic or aromatic derivatives with amino groups diversify this type of ligands. Thus, a variety of mono-, di-, or polifunctional precursors leading to a variety of ligands with different coordination modes can be used.

In this contribution, we have synthesized a novel amine, trimethylsylil-propyl-*p*-aminobenzoate, by using a simple procedure already reported in our previous works [23,24]. The literature study shows several works on homo- and heterometallic complexes of different ligands having trimethylsilyl groups in structure [25–30]. Such compounds have demonstrated amphiphilic character and the ability to self-assemble in solution depending on the solvent polarity [31,32]. These properties may be directed to improving catalytic activity of the complexes in different substrates and to influence the behavior in solution [23]. We have prepared three complexes, one of them with Cu(II) and two with Zn(II), with two bidentate Schiff bases containing trimethylsilyl units in their structure, obtained by condensation reaction of newly synthesized trimethylsilyl-propyl-*p*-aminobenzoate with salicylaldehyde and *o*-vanillin. The obtained compounds were structurally characterized by FTIR, NMR, ESI-MS, elemental analysis and by single crystal X-ray diffraction; their photophysical, thermal and biological properties have been evaluated.

2. Experimental

2.1. Materials

3-Chloropropyltrimethylsilane (Alfa Aesar), *p*-aminobenzoic acid, salicylaldehyde, *o*-vanillin (3-methoxysalicylaldehyde), sodium hydroxide, $CuCl_2{\cdot}2H_2O$, anhydrous $ZnCl_2$, $Zn(ClO_4)_2{\cdot}6H_2O$, dimethylformamide and acetonitrile (Aldrich), triethylamine (Fluka), methanol, ethanol, chloroform, and ethylic ether (Chimopar) were used as received.

2.2. Measurements

Fourier transform infrared (*FT-IR*) *spectra* were recorded on a Bruker Vertex 70 FT-IR spectrometer by using KBr pallets in the transmission mode, in the range 400–4000 cm^{-1} at room temperature with a resolution of 2 cm^{-1}. *The NMR spectra* were recorded on a Bruker Avance DRX 400 MHz Spectrometer equipped with a 5 mm QNP direct detection probe and Z-gradient. Spectra were recorded in $CDCl_3$, at room temperature. The chemical shifts are reported as δ values (ppm) referenced to the solvent residual peak (7.26 ppm). The atom labeling for the NMR assignments is the same as used in the single-crystal X-ray study. The assignments of all signals in the 1D NMR spectra were done using 2D NMR experiments, like H,H-COSY, H,C-HMQC and H,C-HMBC. *Elemental* (*C*, *H*, *N*) compositions were obtained with a Perkin–Elmer CHNS 2400 II elemental analyser. *Electrospray ionisation mass spectra* (ESI-MS) were recorded on a Bruker Esquire 3000 instrument by using methanol as solvent. *UV–Vis absorption* measurements were carried out in DMF solution on a Specord 200 spectrophotometer in a quartz cell with path length of 1.0 cm. *Fluorescence spectra* were obtained by using a Perkin Elmer LS55 luminescence spectrometer in solution in the same cell as the UV. *Thermogravimetric data* were acquired on a STA 449 F1 Jupiter device (Netzsch, Germany). Around 10 mg of each sample was weighed and heated in alumina crucibles, in nitrogen atmosphere at a flow rate of 50 mL min^{-1}. The temperature range was from 30–700 °C with a sample heating rate of 10 °C min^{-1}.

The antimicrobial activity of metal complexes and ligands was assessed on three species of fungi (*Aspergillus fumigatus* ATCC 66567, *Penicillium chrysogenum* ATCC 20044, Fusarium ATCC 20327) from pure culture and two of bacteria (*Pseudomonas sp.* ATCC 15780 and *Bacillus sp*. ATCC 31073). Microorganisms were provided by American Type Culture Collection (ATCC), USA. Culture *in vitro* was performed by the standard procedures (SR-EN 1275:2006 and NCCLS:1993) by using the MIC test strip assay. Caspafugin (small test) was used as a standard compound for antifungal activity and Kanamycin (small test) was used as standard for antibacterial activity. Standard compounds were provided by Liofilchem Company. Cultivation was performed by using 1:1 mixture of microorganism suspension and solution of the compound to be tested. For these determinations, Petri dishes with a culture medium consisting of Sabouraud Agar and Agar-agar from Merck were used. The successive dilution procedure has been used to prepare the suspension of microorganisms. Final load of the prepared stock inoculum was 1×10^{-4} μg/ml. The plates were seeded and incubated at 37 °C. A blank sample was also prepared in order to verify the influence of the solvent on the biological activity. After 24 h of incubation, a symmetrical ellipse of inhibition centered along the strip was formed. The MIC (in μg/mL) was read directly on the scale where the ellipse edge intersects the strip.

2.3. X-ray crystallography

Crystallographic measurements for **2**, **3**, **4,** and **6** were carried out with an Oxford-Diffraction XCALIBUR E CCD diffractometer equipped with graphite-monochromated Mo Kα radiation. Single crystals were positioned at 40 mm from the detector and 337, 221, 218 and 434 frames were measured each for 20, 30, 90, 5 and 60 s over 1° scan width for **2**, **3**, **4** and **6**, respectively. The X-ray data for **5** were collected using an Agilent SuperNova dual wavelength X-ray diffractometer using MoKα radiation. The crystal was positioned at 40 mm from the detector and 502 frames were measured each for 40 s over 1° scan width. The unit cell determination and data integration were carried out using the CrysAlis package of Oxford Diffraction [33]. All the structures were solved by direct methods using Olex2 [34] software with the SHELXS structure solution program and refined by full-matrix least-squares on F^2 with SHELXL-97 [35]. Atomic displacements for non-hydrogen atoms were refined using an anisotropic model. Hydrogen atoms have been placed in fixed, idealized positions accounting for the hybridation of the supporting atoms and the possible presence of hydrogen bonds in the case of donor atoms. The molecular plots were obtained using the Olex2 program. The positional parameters of the DMF and water molecules were refined in combination with PART and SADI tools, available in SHELXL with anisotropic/isotropic model for non-H atoms. Table 1 provides a summary of the crystallographic data together with refinement details for compounds **2**–**6**. CCDC-1062104, 1042105, 1042106, 1042107 and 1042109 contain the

Table 1
Crystallographic data, details of data collection and structure refinement parameters for compounds **2**–**6**.

	2	**3**	**4**	**5**	**6**
Formula	$C_{20}H_{25}NO_3Si$	$C_{21}H_{27}NO_4Si$	$C_{40}H_{48}CuN_2O_6Si_2$	$C_{40}H_{48}ZnN_2O_6Si_2$	$C_{42}H_{58}ZnCl_2N_2O_{18}Si_2$
Formula weight	355.50	385.53	772.52	774.35	1071.35
T (K)	200	173	200	293(2)	293(2)
Crystal system	monoclinic	monoclinic	monoclinic	triclinic	triclinic
Space group	$P2_1/c$	$P2_1/n$	$P2_1/c$	$P\bar{1}$	$P\bar{1}$
a (Å)	21.381(2)	6.2135(5)	12.474(5)	7.6877(12)	7.0475(9)
b (Å)	6.1330(7)	12.0967(7)	9.6362(11)	14.7504(19)	11.1729(15)
c (Å)	15.9342(15)	27.823(2)	17.195(7)	19.129(3)	16.796(3)
α (°)	90	90	90.00	101.318(11)	96.336(13)
β (°)	110.820(11)	93.268(7)	96.76(4)	96.297(12)	93.365(13)
γ (°)	90	90	90.00	99.371(12)	101.615(12)
V (Å^3)	1953.0(3)	2087.8(3)	2052.5(11)	2075.9(5)	1283.1(3)
Z	4	4	2	2	1
D_{calc} (mg/mm^3)	1.209	1.226	1.250	1.239	1.386
μ (mm^{-1})	0.138	0.138	0.636	0.694	0.700
Crystal size (mm^3)	0.80 × 0.15 × 0.05	0.15 × 0.10 × 0.10	0.20 × 0.10 × 0.10	0.5 × 0.05 × 0.02	0.2 × 0.1 × 0.05
θ_{min}, θ_{max} (°)	10.2–52.74	10.22–52.74	5.36–52.74	6.14–47.06	5.78–52.74
Reflections collected	13411	9928	9484	14154	6663
Independent reflections (R_{int})	3985 (0.0747)	4213 (0.0741)	4188 (0.0338)	6154 (0.1141)	6663 (0.0760)
Data/restraints/parameters	3985/0/229	4213/0/249	4188/6/235	6154/0/466	6663/15/298
R_1[a] ($I > 2\sigma(I)$	0.0754	0.0659	0.0667	0.0805	0.0659
wR_2[b] (all data)	0.1311	0.0998	0.1954	0.1923	0.1664
Goodness-of-fit (GOF)[c]	1.052	0.994	1.036	0.968	0.957
Largest difference peak and hole (e Å^{-3})	0.20/−0.24	0.24/−0.26	0.83/−0.54	0.56/−0.30	0.50/−0.43

[a] $R_1 = \Sigma||F_o| - |F_c||/\Sigma|F_o|$.
[b] $wR_2 = \{\Sigma[w(F_o^2 - F_c^2)^2]/\Sigma[w(F_o^2)^2]\}^{1/2}$.
[c] GOF = $\{\Sigma[w(F_o^2 - F_c^2)^2]/(n-p)\}^{1/2}$, where n is the number of reflections and p is the total number of parameters refined.

supplementary crystallographic data for this contribution. These data can be obtained free of charge from the Cambridge Crystallographic Data Centre via www.ccdc.cam.ac.uk/data_request/cif.

2.4. Procedure

2.4.1. Synthesis of trimethylsilyl-propyl-p-aminobenzoate, *1*

A mixture of *p*-aminobenzoic acid sodium salt (2.78 g, 17 mmol) and 3-chloropropyltrimethylsilane (3 mL, 17 mmol) in DMF (20 mL) was heated to reflux for 8 h, then filtered and the obtained filtrate was poured in water, and extracted with chloroform (3 × 50 mL). The organic phase was washed with distilled water (3 × 100 mL). The organic extracts were dried over Na_2SO_4, filtered and concentrated under reduced pressure to afford the compound **1**. Yield: 97%; m.p. 48–50 °C. *Anal.* Calc. for $C_{13}H_{21}NO_2Si$ (M_r 251.39 g/mol): C, 62.11; H, 8.42; N, 5.57. Found: C, 62.24; H, 8.37; N, 5.49. ESI-MS (methanol), positive: *m*/*z* 274.2 ([**1**+Na]$^+$), 524.8 ([2·**1**+Na]$^+$).

IR ν_{max} (KBr), cm^{-1}: 3441m, 3427m, 3352s, 3227m, 2953s, 2887m, 1690vs, 1639s, 1599vs, 1576m, 1516s, 1470m, 1441w, 144vw, 1387m, 313s, 1281vs, 1246s, 1171vs, 1121s, 1084m, 1065w, 1040vw, 995w, 974m, 907vw, 860s, 841s, 772s, 750m, 698m, 638w, 617m, 519m, 505m, 397w.

^{1}H NMR ($CDCl_3$, 400.13 MHz, δ, ppm): 7.87 (d, *J* = 8.4 Hz, 2H, H3, 5), 6.67 (d, *J* = 8.8 Hz, 2H, H2, 6), 4.27 (s, 2H, NH_2), 4.21 (t, *J* = 7 Hz, H8),1.76–1.69 (m, 2H, H9), 0.59–0.54 (m, 2H, H10), 0.01 (s, 9H, H11–13).

^{13}C NMR ($CDCl_3$, 100.6 MHz, δ, ppm): 166.66 (C7), 150.14 (C1), 131.53 (C3, 5), 120.50 (C4), 114.08 (C2, 6), 67.04 (C8), 23.44 (C9), 12.53 (C10), -1.78 (C11–13).

2.4.2. Synthesis of the Schiff base ligands

*2.4.2.1. 3-Trimethylsilyl-1-propyl-4-[(E)-1-(2-hydroxyphenyl)-methylideneamino]benzoat, **HL^A**, **2**.* A mixture of **1** (0.25 g, 1 mmol) and freshly distilled salicylaldehyde (0.12 g, 1 mmol) in methanol/chloroform (2:1 v/v) was stirred to reflux for 4 h and then cooled to room temperature. A yellow solid was formed, which was filtered, washed with methanol and diethyl ether and dried. Crystallization from hot acetonitrile gave **HL^A** (**2**) (0.20 g, 80%); m.p. 82–84 °C. *Anal.* Calc. for $C_{20}H_{25}NO_3Si$ (M_r 355.50 g/mol): C, 67.57; H, 7.09; N, 3.94. Found: C, 67.23; H, 7.14; N, 3.89. ESI-MS (methanol), positive: *m*/*z* 356.1 ([**HL^A**+H]$^+$), 378.1([**HL^A**+Na]$^+$), 732.5 ([2·**HL^A**+Na]$^+$).

IR ν_{max} (KBr), cm^{-1}: 3412vw, 2980w, 2951m, 2899w, 2878w, 1715vs, 1616m, 1599s, 1568s, 1528w, 1506w, 1491m, 1456m, 1443m, 1412m, 1383m, 1366m, 1315m, 1300m, 1267vs, 1248s, 1202m, 1178s, 1150m, 1099s, 1045w, 1030w, 1015w, 999w, 980w, 970w, 957m, 939vw, 912w, 860s, 843s, 789w, 773m, 756s, 692s, 652w, 636vw, 600vw, 517w, 492w, 457vw, 426w.

^{1}H NMR (CDCl3, 400.13 MHz, δ, ppm): 12.81 (s, 1H, –OH), 8.64 (s, 1H, H7), 8.11 (d, *J* = 8.4 Hz, 2H, H10, 12), 7.43–7.39 (m, 2H, H3, 5), 7.31 (d, *J* = 8.4 Hz, 2H, H9, 13), 7.05 (d, *J* = 8.4 Hz, 1H, H2), 6.97 (t, *J* = 7.7 Hz, 1H, H4), 4.29 (t, *J* = 7 Hz, 2H, H15), 1.82–1.74 (m, 2H, H16), 0.62–0.57 (m, 2H, H17), 0.03 (s, 9H, H18–20).

^{13}C NMR ($CDCl_3$, 100.6 MHz, δ, ppm): 166.10 (C14), 164.09(C7), 161.27(C1), 152.32 (C8), 133.85 (C3), 132.66 (C5), 131.01 (C10, 12), 128.78 (C11), 121.11 (C9, 13), 119.30 (C4), 118.94 (C6), 117.40 (C2), 67.72 (C15), 23.40 (C16), 12.53 (C16), −1.77 (C18–20).

*2.4.2.2. 3-Trimethylsilyl-1-propyl-4-[(E)-1-(2-hydroxy-3-metoxyphenyl)methylideneamino]benzoat, **HL^B**, **3**.* A mixture of **1** (0.25 g, 1 mmol) and *o*-vanillin (0.15 g, 1 mmol) in methanol/chloroform (5 mL, 2:1 v/v) was stirred at room temperature for 4 h and, then heated to reflux for 2 h. A red precipitate appeared which was filtered, washed with methanol and diethyl ether and dried. Crystals of **HL^B** (**3**) were obtained by recrystallization from acetonitrile (0.19 g, 76%); m.p. 95 °C. *Anal.* Calc. for $C_{21}H_{27}NO_4Si$ (M_r 385.53 g/mol): C, 65.42; H, 7.06; N, 3.63. Found: C, 65.53; H, 7.11; N, 3.72. ESI-MS (methanol), positive: *m*/*z* 386.2 ([**HL^B**+H]$^+$), 417.1([**HL^B**+MeOH]).

IR ν_{max} (KBr), cm^{-1}: 3410vw, 2953m, 2928w, 2893w, 2872w, 2835w, 1719vs, 1616m, 1593s, 1572s, 1503w, 1466s, 1443m, 1412m, 1383w, 1362m, 1339w, 1310m, 1273vs, 1254vs, 1200m, 1167s, 1113s, 1078m, 1011w, 989w, 968s, 858s, 845s, 833s, 783m, 758w, 748w, 733s, 694m, 669w, 581w, 571w, 413w.

^{1}H NMR ($CDCl_3$, 400.13 MHz, δ, ppm): 13.31 (s, 1H, –OH), 8.64 (s, 1H, H8), 8.11 (d, J = 8.4 Hz, 2H, H11, 13), 7.31 (d, J = 8.4 Hz, 2H, H10, 14), 7.05–7.01 (m, 2H, H3, 5), 6.90 (t, J = 7.8 Hz, 1H, H4), 4.29 (t, J = 7 Hz, 2H, H16), 3.94 (s, 3H, H7), 1.81–1.73 (m, 2H, H17), 0.61–0.57 (m, 2H, H18), 0.03 (s, 9H, H9–21).

^{13}C NMR ($CDCl_3$, 100. 6 MHz, δ, ppm): 166.07 (C15), 164.09 (C8), 152.10 (C9), 151.50 (C1), 148.50 (C2), 131.00 (C11, 13), 128.82 (C12), 124.03 (C5), 121.10 (C10, 14), 118.89 (C6), 118.79 (C4), 115.27 (C3), 67.69 (C16), 56.20 (C7), 23.38 (C17), 12.52 (C18), -1.78 (C19–21).

2.4.3. Synthesis of complexes

2.4.3.1. Bis{3-trimethylsilyl-1-propyl-4-[(E)-1-(2-phenoxy)methylideneamino]benzoat}Copper(II), ***[Cu(L^A)$_2$]***, ***4***. A methanolic solution (5 mL) of $CuCl_2{\cdot}2H_2O$ (0.17 g, 1 mmol) was added dropwise to a solution of **HL^A** (0.36 g, 1 mmol) in methanol/chloroform solvent mixture (5 mL). Few drops of triethylamine were added, and the mixture was stirred for 2 h at 50 °C. The solution turned dark brown. Crystals of **4** were formed after two weeks by slow evaporation of the mixed solvents at room temperature. The crystals were washed with methanol and diethyl ether and dried (0.26 g, 33%). m.p. 65 °C. *Anal.* Calc. for $C_{40}H_{48}N_2O_6Si_2Cu$ (M_r 772.52 g/mol): C, 62.19; H, 6.26; N, 3.63. Found: C, 62.24; H, 6.18; N, 3.66. ESI-MS (methanol), positive: m/z 772.2 ([**Cu(L^A)$_2$**]), 796.2 ([**Cu(L^A)$_2$**+Na]$^+$).

IR ν_{max} (KBr), cm^{-1}: 3387w, 3076vw, 2951m, 2891m, 1699vs, 1612s, 1599vs, 1568s, 1541m, 1506w, 1491m, 1468m, 1447m, 1414m, 1379m, 1350vw, 1319s, 1279vs, 1246s, 1180s, 1150s, 1126s, 1113s, 1063w, 1030w, 1015w, 991w, 961m, 912m, 856s, 839vs, 772s, 758s, 694s, 636w, 600w, 590w, 582w, 561vw, 526w, 517w, 492w, 447w, 405w.

2.4.3.2. Bis{3-Trimethylsilyl-1-propyl-4-[(E)-1-(2-phenoxy)methylideneamino]benzoat}Zinc(II), ***[Zn(L^A)$_2$]***, ***5***. Zn(II) complex was prepared according to the same synthetic procedure reported for **4** starting from **HL^A** (0.36 g, 1 mmol) and anhydrous $ZnCl_2$ (0.14 g, 1 mmol) in the same solvent mixture. Crystals of **5** were obtained after two days by slow evaporation of the mixed solvents at room temperature. The crystals were washed with methanol and diethyl ether and dried (0.25 g, 32%). m.p. 180 °C. *Anal.* Calc. for $C_{40}H_{48}N_2O_6Si_2Zn$ (M_r 774.35 g/mol): C, 62.04; H, 6.25; N, 3.62. Found: C, 62.34; H, 6.28; N, 3.61. ESI-MS (methanol), positive: m/z 773.3 ([**Zn(L^A)$_2$**]), 797.2 ([**Zn(L^A)$_2$**+Na]$^+$).

IR ν_{max}(KBr), cm^{-1}: 3422vw, 3078w, 3061vw, 3020vw, 2982vw, 2949m, 2893w, 2874w, 1707vs, 1612s, 1601s, 1585vs, 1531s, 1506m, 1462s, 1439vs, 1396s, 1354m, 1329m, 1315m, 1275vs, 1250s, 1221w, 1173vs, 1148vs, 1124m, 1107s, 1045w, 1032m, 1016m, 1005w, 993w, 984w, 962w, 928w, 853s, 839s, 793w, 783w, 760s, 752s, 692m, 588w, 575w, 521w, 488w, 457vw, 444vw, 380vw.

2.4.3.3. Diaqua-bis{3-Trimethylsilyl-1-propyl-4-[(E)-1-(2-hydroxy-3-metoxyphenyl)methylideneamino]benzoat}Zinc(II), ***[Zn(L^B)$_2$(H$_2$O)$_2$]2ClO$_4$***, ***6***. A methanolic solution (5 mL) of $Zn(ClO_4)_2{\cdot}6H_2O$ (0.37 g, 1 mmol) was added dropwise to a solution of **HL^B** (0.38 g, 1 mmol) in methanol (5 mL). The mixture was stirred for 24 h at 50 °C, and then evaporated at room temperature. After one week, crystals of **6** were formed that have been washed with methanol and diethyl ether and dried (0.28 g, 27%). m.p. 125 °C. *Anal.* Calc. for $C_{42}H_{58}N_2O_{18}Si_2ZnCl_2$ (M_r 1071.35 g/mol): C, 47.09; H, 5.46; N, 2.62. Found: C, 48.13; H, 5.61; N, 2.49. ESI-MS (methanol), positive: m/z 833.3 ([**Zn(L^B)$_2$**]).

IR ν_{max} (KBr), cm^{-1}: 3377m, 3082vw, 3049vw, 2982vw, 2949m, 2891w, 2847vw, 1693s, 1634vs, 1603s, 1553m, 1501s, 1458m, 1439m, 1429w, 1394w, 1369m, 1346w, 1329m, 1290s, 1248s, 1236s, 1194s, 1169vs, 1126vs, 1113vs, 1072s, 1047s, 1013m, 989vw, 974vw, 959m, 949m, 903w, 868s, 851s, 841s, 787m, 768m, 746s, 735s, 687m, 665w, 623s, 575w, 527m, 496m, 449w, 430w, 417w.

3. Results and discussion

The Schiff base ligands **2** and **3** were synthesized by the direct condensation reaction of trimethylsilyl-propyl-*p*-aminobenzoate **1** with two aldehydes, salicylaldehyde and *o*-vanillin, respectively (Scheme 1(a)), their structures being confirmed by single crystal X-ray diffraction analysis. The complexation behavior of the synthesized ligands **2** and **3** toward Cu(II) and Zn(II) ions was investigated and three new complexes were obtained. Complexes **4** and **5** were prepared by mixing the ligand **2** with $CuCl_2{\cdot}2H_2O$ and $ZnCl_2$, respectively, in 1:1 molar ratio in methanol/chloroform solvent mixture, while **6** was obtained by reaction of ligand **3** with $Zn(ClO_4)_2{\cdot}6H_2O$ in methanol (Scheme 1(c)).

All the synthesized compounds are soluble in polar and nonpolar solvents such as methanol, ethanol, acetonitrile, THF, DMF, DMSO, $CHCl_3$ or CH_2Cl_2.

3.1. FTIR analysis

The IR spectra of the compounds **1**–**6** can be seen in Figs. 1S–3S. The spectrum of the amine **1** exhibits strong absorption bands at 3427, 3352 and 3227 cm^{-1} assigned to the ν(NH$_2$) and at 1690 cm^{-1} attributed to the ν(C=O) absorption of the ester group. The characteristic absorption bands for trimethylsilyl groups appear at 1246 and 841 cm^{-1} (Fig. 1S). The absence of the characteristic amino and carbonyl stretching bands in the spectra of the Schiff base ligands and the appearance of the imine –CH=N– band at 1616 cm^{-1} clearly indicate Schiff base formation. The ν(C=O) absorption of the ester group in the spectra of the ligands is shifted at higher wavenumber towards amine, from 1690 cm^{-1} to 1715 cm^{-1} (**2**) and 1719 cm^{-1} (**3**). The specific bands for –Si–CH$_3$ groups appear at 1248 and 843 cm^{-1} (**2**), 1254 and 845 cm^{-1} (**3**). In the IR spectra of the Cu(II) and Zn(II) complexes **4** and **5** of the Schiff base **2**, the imine band is shifted by 2–4 cm^{-1} to lower frequencies due to the withdrawal of electron density from the nitrogen atom owing to coordination (Fig. 2S) [36], while in the IR spectrum of the Zn(II) complex **6** of the Schiff base **3**, the imine band is shifted to 1634 cm^{-1} suggesting that coordination does not occur through the nitrogen atom from the azomethyne bond (Fig. 3S).

The crystal data also confirm the lack of coordination by the nitrogen atom in this complex. New bands in the region 550–370 cm^{-1} were attributed to characteristic vibrations associated with M–N and M–O bonds, respectively [37,38].

3.2. NMR analysis

The 1D and 2D NMR spectra of the amine **1** and Schiff base ligands (**2** and **3**) are given in Figs. 4S–18S. The ^{1}H NMR of the amine **1** exhibited two signals at 7.86 and 6.67 ppm attributed to aromatic protons, a broad peak for the two amino protons at 4.27 ppm, partially overlapping with the triplet at 4.21 ppm assigned to –CH$_2$–O–, while the peaks corresponding to the –CH$_2$– and –Si–CH$_3$ protons appear between 1.76 ppm and 0.01 ppm (Fig. 4S). ^{13}C NMR spectrum also confirmed the proposed structure (Fig. 5S). In the ^{1}H NMR spectra of the Schiff base ligands, all protons resonated at appropriate positions: a singlet for –OH protons at 13.31 ppm (**3**) and 12.81 ppm (**2**), a singlet for azomethine hydrogen (–CH=N–) at 8.64 ppm (**2** and **3**), aromatic protons shifted to 8.12–6.95 ppm (**2**) and to 8.12–6.88 ppm (**3**), a singlet at 3.94 ppm for the methoxy group (**3**), while aliphatic protons

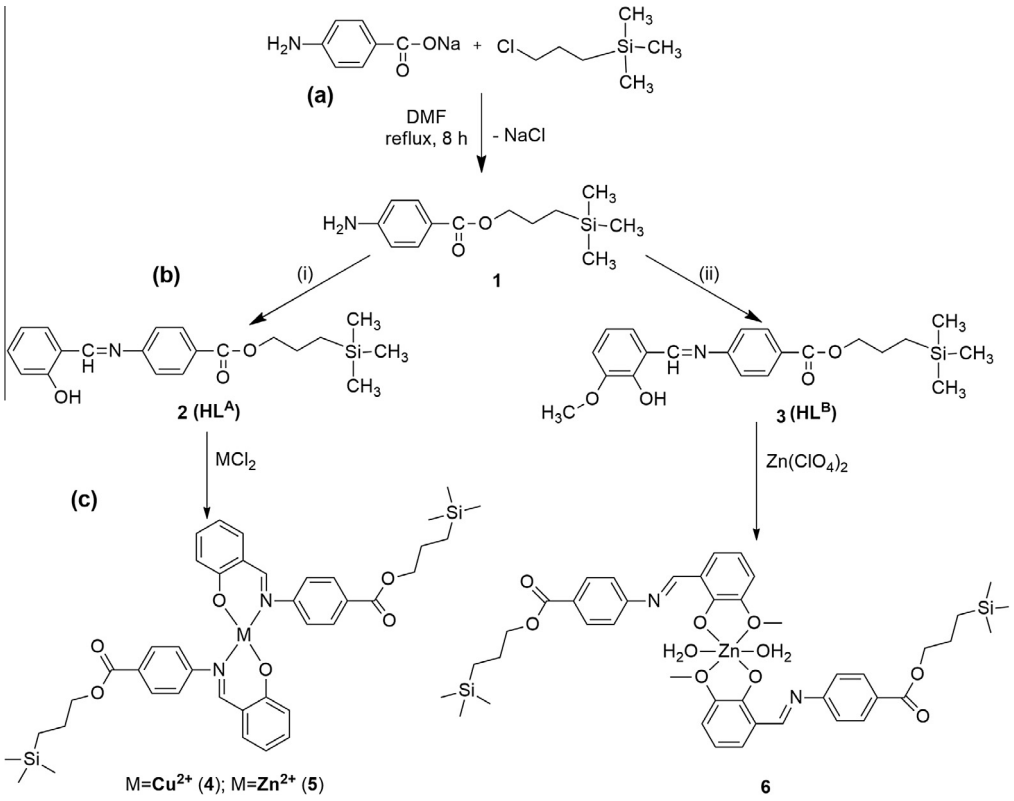

Scheme 1. Reaction pathways for obtaining the new amine **1** (a), Schiff base derivatives (b) and metal complexes (c).

appear in the region 4.35–0.57 ppm and those of trimethylsilyl groups appear at 0.07–0.03 ppm (Figs. 9S and 14S). The structures of the ligands were also confirmed by ^{13}C NMR spectra (Figs. 10S and 15S).

3.3. ESI-MS spectra

The synthesized compounds **1**–**6** were characterized by ESI-MS spectrometry in the positive ion mode. ESI-MS spectra of the trimethylsilyl-propyl-*p*-aminobenzoate and its Schiff bases in methanol showed intense peaks related to [**1**+Na]$^+$, [2·**1** +Na]$^+$ fragments (Fig. 19S), to [**HL^A**+H]$^+$, [**HL^A**+Na]$^+$, [2·**HL^A**+Na]$^+$ fragments (Fig. 20S) and to [**HL^B**+H]$^+$, [**HL^B**+MeOH] fragments (Fig. 21S), respectively. Also it has been possible to detect the molecular peaks for the synthesized complexes. Thus, ESI-MS spectra indicated intense peaks due to [**Cu(L^A)$_2$**], [**Cu(L^A)$_2$**+Na]$^+$, [**Zn(L^A)$_2$**], [**Zn(L^A)$_2$**+Na]$^+$and [**Zn(L^B)$_2$**] fragments, respectively (Figs. 22S–24S).

3.4. X-ray crystallography

The single-crystal X-ray investigation has demonstrated the molecular structure of the studied Schiff bases, which consists of neutral entities without any cocrystallized solvent molecules. The molecular structure and atom numbering scheme for compounds **2** and **3** are shown in Figs. 1 and 2, while the bond distances and angles are summarized in Tables 1S and 2S (see Fig. 3).

The crystal packing of **2** and **3** is predominantly stabilized by π–π stacking interactions, as shown in Figs. 3 and 25S. Thus, in the crystal structure of **2**, *Cg*1 (the centroid of the C1–C6 ring) and *Cg*2 (the centroid of the C8–C13 benzene ring) of the symmetrically related unit forms a π–π stacking interaction, with a centroid-to-centroid distance of 3.650 Å and shift distance of

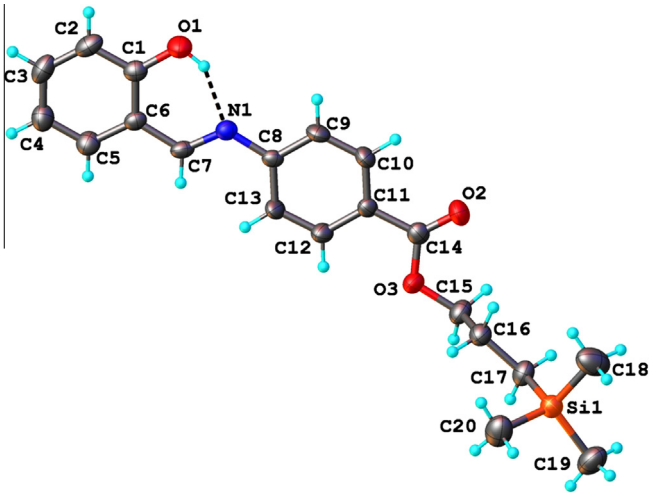

Fig. 1. X-ray molecular structure of **HL^A** (**2**) showing the atom-numbering scheme. The thermal ellipsoids are drawn at 50% probability level. H-bonds: O1–H···N1 [O1–H 0.82 Å, H···N1 1.87 Å, O1···N1 2.597(3) Å, O1–H···N1 147.4°].

1.051 Å [symmetry code: (*i*) –*x*, 3–*y*, –1–*z*]. These interactions determine the formation of the columns (Fig. 4) in parallel packing along the *b* crystallographic axis (Fig. 25S). The main crystal structural motif in **3** is characterized as a one-dimensional arrangement along [1 0 1], sustained through π–π stacking interactions. This is evidenced by the *Cg*1···*Cg*2^i intermolecular short contact of 3.745 Å and 1.299 Å shift distance [symmetry code: (*i*) 1+*x*, *y*, *z*], as shown in Fig. 4.

Based on X-ray crystallography, coordination compounds **4** and **5** have a mononuclear molecular structure of general formula [M(L^A)$_2$] comprising M = Cu^{2+}, respectively Zn^{2+} metal ions and

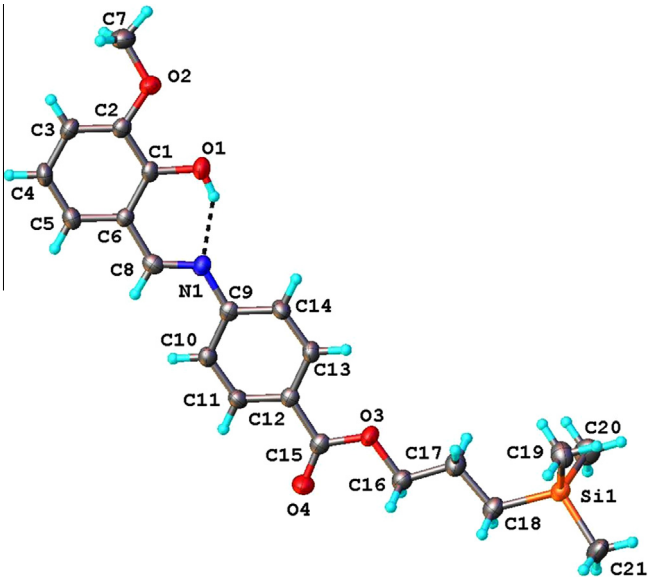

Fig. 2. X-ray molecular structure of HL^B (**3**) showing the atom-numbering scheme. The thermal ellipsoids are drawn at 50% probability level. H-bonds: O1–H···N1 [O1–H 0.82 Å, H···N1 1.88 Å, O1···N1 2.605(3) Å, O1–H···N1 147.2°].

two deprotonated L^{A-} ligands, as depicted in Figs. 5 and 6. The bonds distances and angles are summarized in Tables 3S and 4S. The asymmetric unit in the crystal of **4** contains one half of the molecule (Fig. 5) with the other half generated by an inversion center which lies on the position of copper atom. The Cu^{2+} ion is coordinated by two N atoms at 2.005(3) Å and two O atoms at 1.868(3) Å, which form, as expected, a strict square-planar geometry for the CuN_2O_2 coordination core. The bond angles around the Cu1 atom range between 88.5(1)° and 91.5(1)°. The six-membered chelating ring (Cu1, O1, C1, C6, C7, N1) and the benzene ring are almost co-planar with a mean deviation of 0.039(4) Å.

On the contrary, the ZnN_2O_2 coordination environment in $[Zn(L^A)_2]$ (**5**) (Fig. 6) forms a distorted tetrahedral geometry, with average bond distances Zn1–N = 2.000(6) Å, Zn1–O = 1.906(6) Å and angles subtended at the Zn^{II} atom in the range of 95.7(2)–121.8(2)° (Table 1S). Two asymmetric six-membered chelating rings (Zn1, O4, C21, C26, C27, N2) and (Zn1, O3, C20, C15, C14, N1) along with their adjacent benzene rings are also almost co-planar with a mean deviation of 0.046(4) Å and 0.034(4) Å, respectively.

The crystal structure of **4** is built up from discrete, weakly interacting $[Cu(L^A)_2]$ neutral molecules. In the crystal **5** $Cg1\cdots Cg2^i$ [symmetry code: (i) $2-x, -y, 1-z$] π–π contacts between benzene rings with centroid–centroid of 3.666 Å and shift of 1.191 Å distances determined the formation of the centrosymmetric dimer associates as the main packing unit. A view of this dinuclear associate is shown in Fig. 7.

The results of X-ray diffraction study of complex **6** together with atomic numbering scheme are shown in Fig. 8. The crystal has an ionic structure consisting from mononuclear complex cations $[Zn(L^B)_2(H_2O)_2]^{2+}$ and ClO_4^- anions. No water molecules of crystallization have been found in the crystal.

Each $[Zn(HL^B)_2(H_2O)_2]^{2+}$ cation sits on a crystallographic inversion center and comprises two HL^B ligands and two water molecules. The Zn atom is located on the inversion center and shows a quite regular (O_6) coordination polyhedron. All the Zn1–O bond distances vary from 2.001(3) Å to 2.156(3) Å, while O–Zn1–O angles from 88.9(1)° to 91.1(1)°. Two HL^B molecules behave as bidentate non-deprotonated ligands forming the equatorial square planar (O_4) donor set. The amine N atoms of the Schiff base ligands are protonated and take no part in the coordination to the Zn^{II} ion. The position of this proton was determined on the difference Fourier map and was refined according to the parameters of the H-bond towards the O1 atom as acceptor (Fig. 8). The octahedral geometry of Zn atom is completed by two trans aqua ligands at axial positions, so that the charge balance is in agreement with the formation of species $[Zn(HL^B)_2(H_2O)_2]2(ClO_4)$ for compound **6**. The bond distances and angles are summarized in Table 5S. In the crystal **6**, the apical coordinated water molecules function as hydrogen-bond donors to the carboxylic group and non-coordinated counter-anion ClO_4^-. Apart from H-bonding, the π–π contacts between the benzene rings $Cg1\cdots Cg2^i$ [symmetry code: (i) $1-x, -1-y, 1-z$] of 3.822 Å, where $Cg1$ and $Cg2$ are the centroids of the rings C1–C6 and C10–C14, are further effective in the stabilization of the crystal packing. Weak hydrogen bonds C8-H···O6 [H···A = 2.51 Å, DHA = 166.5°], C10–H···O6

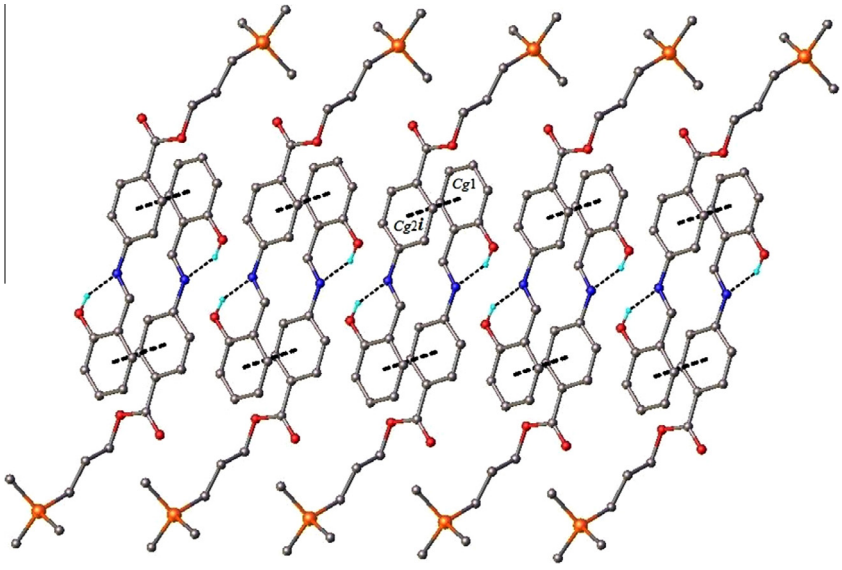

Fig. 3. π–π stacking interactions in the crystal structure of **2**.

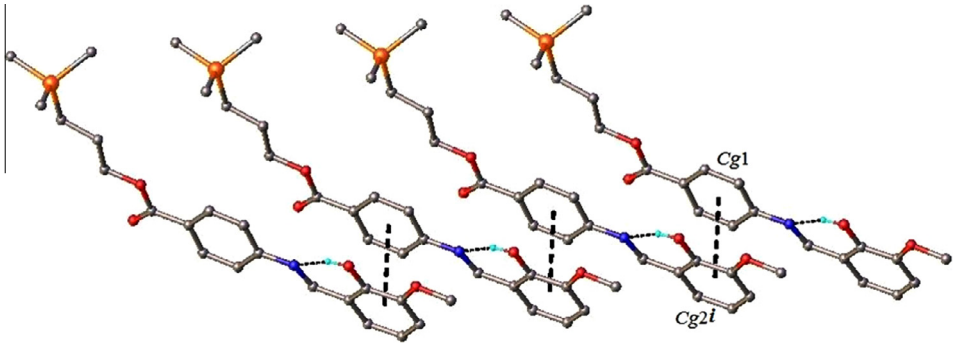

Fig. 4. A view of one-dimensional supramolecular chain in crystal structure of **3**, formed *via* stacking interactions. *Cg*1 and *Cg*3 are the centroids of C1–C6 and C9–C14 rings, respectively.

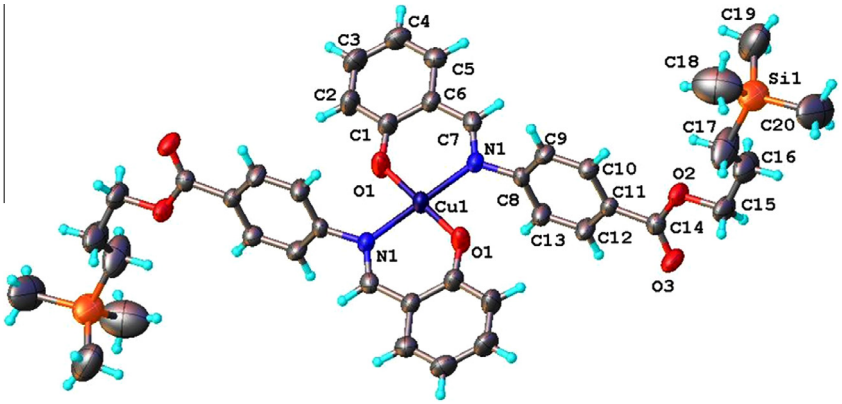

Fig. 5. X-ray molecular structure of $[Cu(L^A)_2]$ (**4**) showing the atom-numbering scheme. The thermal ellisoids are drawn at 50% probability level.

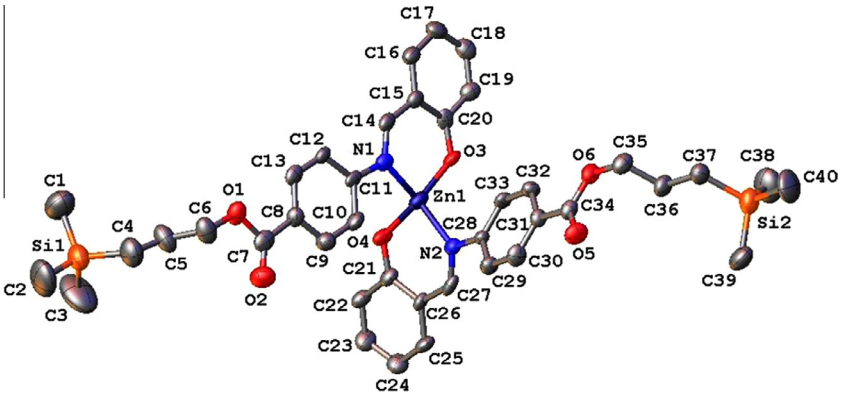

Fig. 6. X-ray molecular structure of $[Zn(L^A)_2]$ (**5**) showing the atom-numbering scheme. The thermal ellipsoids are drawn at 40% probability level.

[H···*A* = 2.67 Å, *DHA* = 162.2°] and C10–H···O8 [H···*A* = 2.50 Å, *DHA* = 144.9°] are also observed. Altogether these intermolecular interactions generate a three-dimensional supramolecular architecture, as shown in Fig. 9.

3.5. Photophysical properties

The absorption spectra of the amine containing trimethylsilyl groups and the resulting Schiff base ligands and complexes were investigated in DMF solution. Fig. 10 presents the absorption and emission spectra of un-complexed Schiff bases **2** and **3** in comparison with their corresponding metal complexes **4**, **5** and **6**. The photophysical data are listed in Table 2. The first excited singlet state S1(π^*, π) of the enolic form shows a stable position of its absorption maximum in **2** and derived complexes (Fig. 10 (a)), and a pronounced decreasing of its extinction coefficient as a result of the introduction of methoxy group in **3** (Fig. 10 (b)). The different profile of the absorption spectrum in the **3** series is given by the partially replacement of the intramolecular OH···N by the OH···OH-bond. The spectra of the metal complexes exhibit a tail beyond 350 nm, which is attributed to a combination of π–π^* transitions of the imine chromophore and ligand to metal charge transfer (LMCT) [35–38].

Schiff base complexes are promising materials for optoelectronic applications, their synthetic flexibility leading to the optimization of the structures through minor changes of their

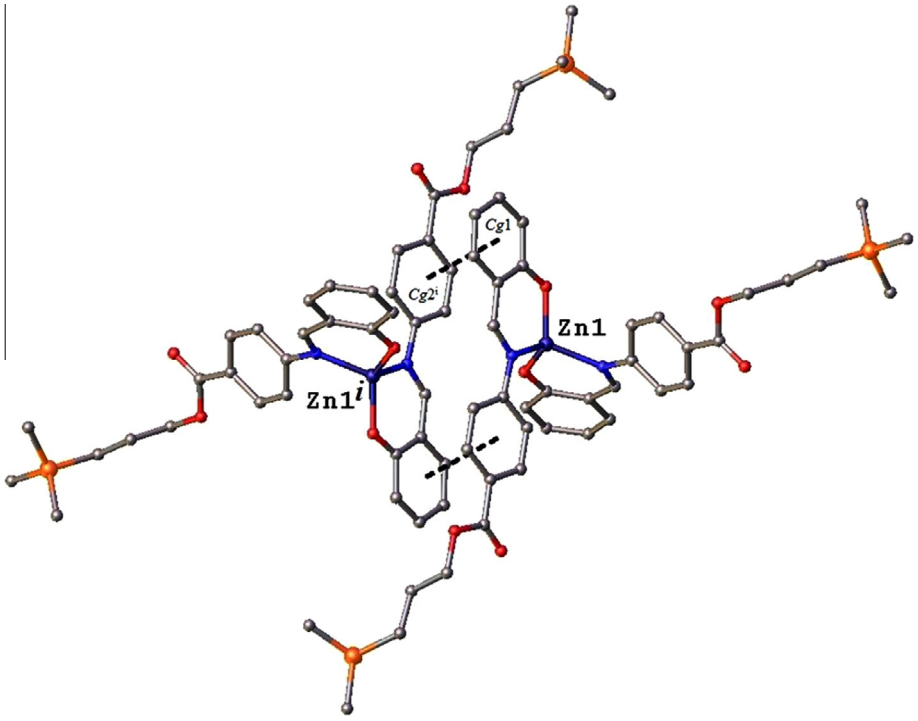

Fig. 7. π–π interaction in the crystal structure $[Zn(L^A)_2]$ (**5**). *Cg*1 and *Cg*2 are the centroids of C15–C20 and C8–C13 rings, respectively.

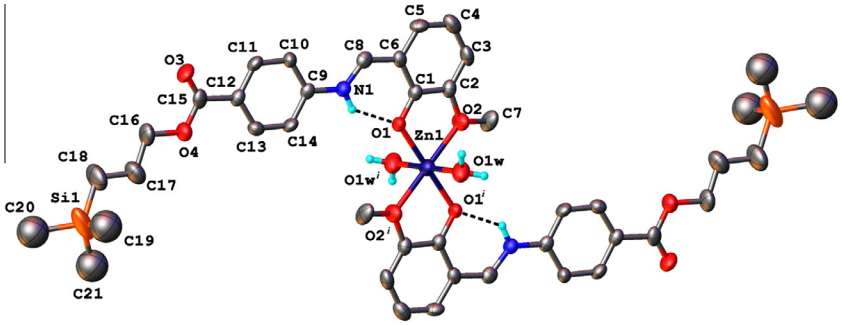

Fig. 8. X-ray structure of $[Zn(L^B)_2(H_2O)_2]^{2+}$ (**6**) with thermal ellisoids are drawn at 50% probability level. H-bond: N1–H···O1 [N1–H 0.86 Å, H···O1 1.94 Å, N1···O1 2.617(4) Å, N1–H···O1 135.1°].

functionalities. A special importance was given to the use of metals with d^{10} electronic configuration, Zn, because of their special properties (chemical, physical, catalytic and optical) and versatility of luminescent properties [39,40]. Beside them, those based on copper ions, with d^9 electronic configuration are also of interest. Luminescent copper(II) and zinc(II) complexes received a special attention due to their applications in different fields, such as chemical sensors, organic light-emitting diodes (OLEDs), light-emitting electrochemical cells (LECs) [40].

For the **2** and **3** ligands, the emission spectra show very weak and dual emission characteristics. The normal emission from the enol tautomer is observed around 410 nm in **2** and 430 nm in **3**, in the last case being red-shifted due to the electron donating ability of the $-OCH_3$ group. The second contribution with a much lower intensity is largely Stokes shifted with respect to the enol absorption band (≈10,520 cm^{-1} for **2** and ≈11,620 cm^{-1} for **3**) and proves the occurrence of an ultrafast proton transfer process in the two ligands. The complexes are more fluorescent and their emission bands are broader than those of the ligands. Complexation of the ligand **2** leads to the stabilization of the tautomeric form, thus the violet fluorescence (410 nm) from the excited enol species is the most important part of the emission in complex **4**. Coordination to the Zn atom in **5** led to the stabilization of the *cis*-keto* structures, which de-activate through a green emission (516 nm). In contrast, the **6** complex with the *o*-vanillin moiety have a blue-shifted keto emission in the emerald green region (545 nm). The main emission from the deep blue region (438 nm) is enhanced, but the general appearance of the fluorescence spectrum is similar to that of the ligands. Irrespective of the substitution pattern, the impact of the coordination is seen by an increase in the intensity of the emission for both compounds, because of the increased rigidity of the structure around the coordination site that minimizes the non-radiative relaxation.

3.6. Thermal analysis

The TG and DTG curves of the compounds **1**–**6** are shown in Fig. 11, while in Table 3 are centralised the main data. For the starting amine and its azomethines, the decomposition process takes place in one step, with a maximum weight loss in the range

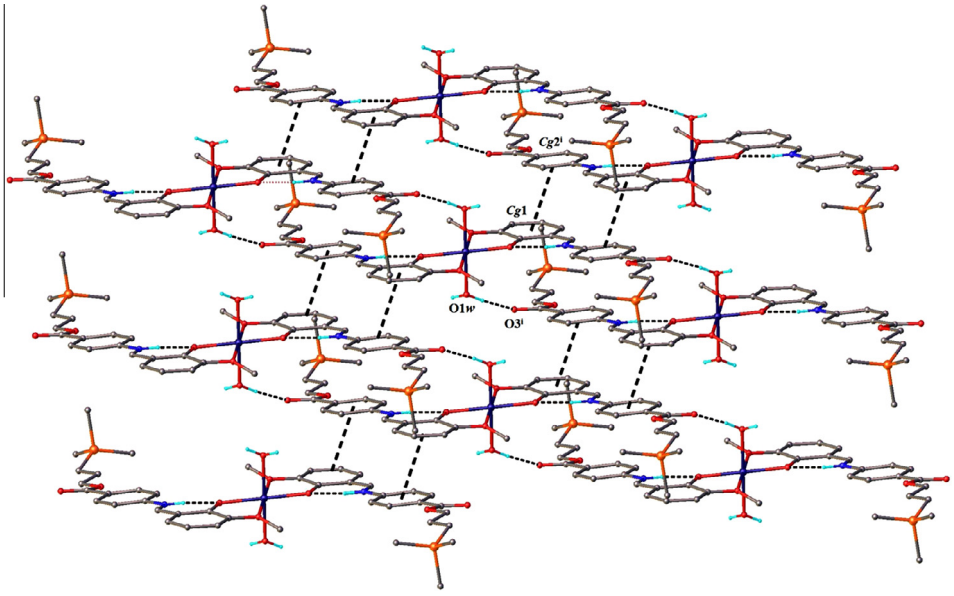

Fig. 9. A view of three-dimensional network in the crystal structure of $[Zn(HL^B)_2(H_2O)_2]2ClO_4$ (**6**). Out-of-sphere ClO_4^- anions are omitted for clarity. H-bonds parameters: O1*w*–H···O3 [O1*w*–H 0.85 Å, H···O3 1.87 Å, O1*w*···O3 2.707(5) Å, O1*w*–H···O3 168.3°]; O1*w*–H···O8 [O1*w*–H 0.86 Å, H···O8 1.98 Å, O1*w*···O8 2.812(5) Å, O1*w*–H···O8 161.4°].

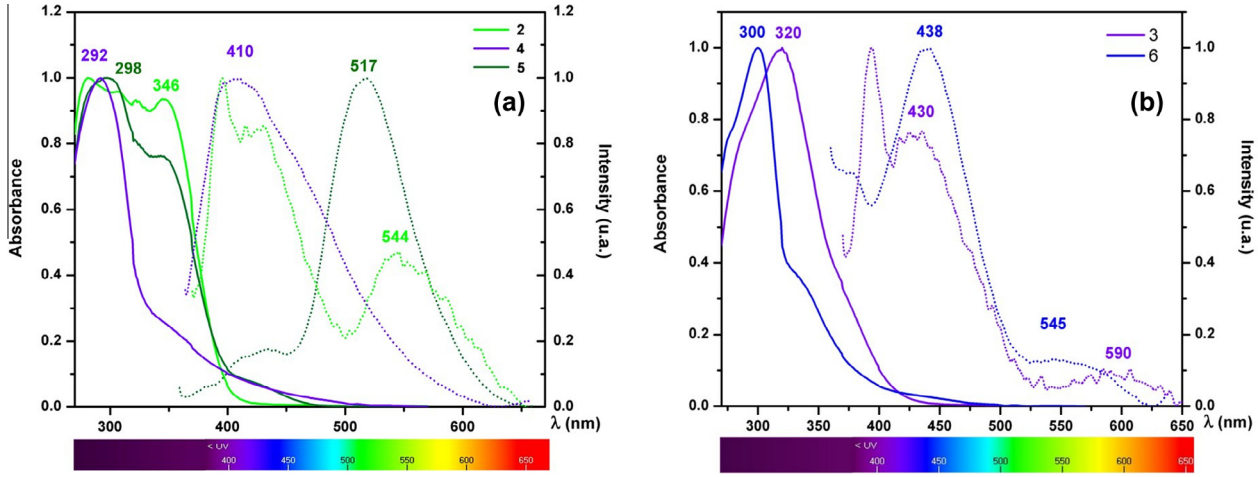

Fig. 10. Normalized electronic absorption and fluorescence spectra of the Schiff base ligands (**2** and **3**) and metal complexes (**4**, **5** and **6**) in dimethylformamide solution ($c = 1.54 \times 10^{-5}$ mol L^{-1}). The emission spectra were recorded at $\lambda_{exc} = 350$ nm, which corresponds to the $S_1 \leftarrow S_0(\pi^*, \pi)$ electronic transition in imine moiety.

Table 2
Spectral data of the compounds **1**–**6** in DMF solution.

Compound	Absorption			Emission	
	λ_{max}, nm (ε, L Mol^{-1} cm^{-1})			λ_{em1} [a]	λ_{em2} [b]
1	298 (31000)			–	–
2	282 (44830)	324 (32897)	346 (22778)	410	544
3	320 (45213)			430	590
4	292 (46912)	348 (36294)		410	–
5	298 (40950)	344 (31160)	420 (4220)	434	–
				517	
6	300 (51930)	335(19210)	440 (1560)	438	550
				545	

[a] $\lambda_{exc} = 340$ nm.
[b] $\lambda_{exc} = 430$ nm.

321–379 °C, assigned to the organic moieties loss. For all the complexes, the process of the decomposition occurs in multiple stages: a slight mass loss (2–4%) in the range 108–271 °C attributed to the loss of solvent molecules and water of crystallization, a maximum weight loss (20–62%) in the range of 248–339 °C corresponding to the loss of ligand moiety and coordinated water, and a slow mass loss in the range of 290–500 °C for complexes **5** and **6** corresponding to a total decomposition of the ligand, with total residues in the range 33–54% (Table 3). A lower stability of the metal complexes was observed. A significant contribution to this behavior can be attributed to the coordination geometry of the metal ion, and to other factors: solvent polarity, the stoichiometric ratio of the ligand and metal ion, intermolecular interactions (coordinative bonds, H-bonds, π–π stacking interactions, etc.) or the catalytic action of the metal ion in the decomposition process [41,42].

3.7. Antimicrobial and antifungal activity

The biological activity of the Schiff base is mainly due to the presence of the azomethine group in the structure, while in the

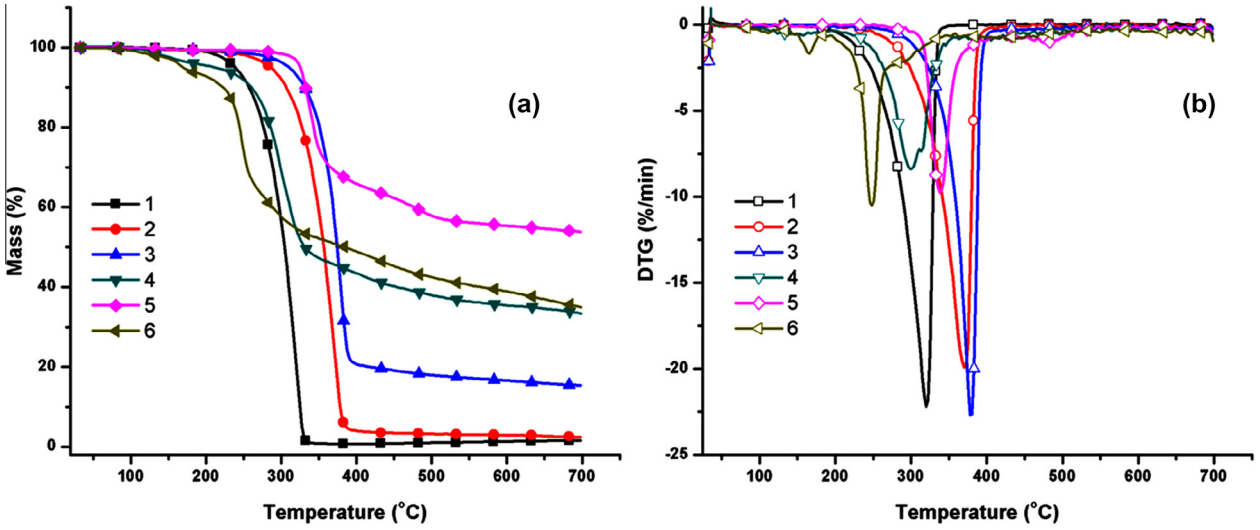

Fig. 11. TG (a) and DTG (b) curves of the compounds **1**–**6**.

Table 3
Thermal characteristics extracted from TG and DTG curves.

Compound	Stage	T_{onset} (°C)	T_{max} (°C)	T_{endset} (°C)	W_m (%)	W_{rez} (%)
1	I	221	321	333	97	2
2	I	255	371	383	97	2
3	I	294	379	392	83	15
4	I	108	157	176	4	33
	II	231	300; 314	331	62	
5	I	271	286	320	2	54
	II	320	339	371	34	
	III	457	474	508	10	
6	I	156	165	173	4	33
	II	201	248	257	21	
	III	257	292	313	17	
	IV	385	426	464	16	

T_{onset} – the temperature at which the thermal degradation begins.
T_{max} – the temperature that corresponds to the maximum rate of decomposition for each stage evaluated from the peaks of the first derivative (DTG) curves.
T_{endset} – the temperature at which the process ends.
W_m – the mass loss corresponding to T_{max} values.
W_{rez} – the percent of residue at the end of thermal degradation (700 °C).

case of the metal complexes the biological activity depends on the coordination mode and the nature of the metal ion [43]. The copper and zinc complexes are known for their biological activities [43–46]. The compounds **1**–**6** were tested as antimicrobial agents *in vitro*, using three species of fungi (*A. fumigatus* ATCC 66567, *P. chrysogenum* ATCC 20044, Fusarium ATCC 20327) and two bacteria (*Bacillus sp.* ATCC 31073, *Pseudomonas sp.* ATCC 15780). The results of the antimicrobial and antifungal activities were compared against DMF as the blank test and the standard compounds (Caspofungin and Kanamycin) and are expressed as values of minimum inhibitory concentration (MIC, μg/ml) in Table 4.

The antimicrobial activities of the Schiff bases **2** and **3** can be explained by their ability in the formation of hydrogen bonds through N and O donor atoms with the cellular constituents. The most active among the tested samples was compound **3**, its structure with the methoxy group in *ortho* position of the benzene seems to be the major factor influencing the biological activity. The presence of the Cu(II) ions, as in the case of complex **4**, contributes to the increasing of the biological activity compared to the corresponding ligand **2** (Table 4), due to its lipophilic character [47]. A different behavior was observed in Zn(II) complex (**6**) with a lower biological activity in comparison with the ligand **3**. This is attributed to the coordination mode of the Zn(II) ions through oxygen atoms from the methoxy group (Fig. 9). The results of the tests indicated a higher antifungal activity for the Schiff bases and their complexes as compared with standard compound Caspofungin, and a good antibacterial activity of the Schiff base **3** and its Zn(II) complex (**6**) in comparison with the standard compound Kanamycin.

Table 4
Antimicrobial and antifungal screening results.

Compound	MIC (μg/ml)				
	Fungi			Bacteria	
	Aspergillus fumigatus ATCC 66567	*Penicillium chrysogenum* ATCC 20044	Fusarium ATCC 20327	*Bacillus sp.* ATCC 31073	*Pseudomonas sp.* ATCC 15780
1	1.5	1.5	1.5	48	48
2	0.19	0.19	0.19	1.5	1.5
3	0.016	0.016	0.016	0.38	0.38
4	0.064	0.064	0.064	1	1
5	0.75	0.75	0.75	32	32
6	0.047	0.047	0.047	0.50	0.50
Caspofungin[a]	0.3	0.3	0.3		
Kanamycin[a]				4	4

[a] Standard compound.

4. Conclusions

Three complexes of copper(II) (**4**), and zinc(II) (**5** and **6**), with bidentate O,N-donor Schiff bases derived from salicylaldehyde and *o*-vanillin (**2** and **3**) and a new amino derivative containing trimethylsilyl groups in the structure, have been synthesized and structurally characterized. Single crystal X-ray studies showed various patterns in coordination geometry of the metal ions leading to discrete or 3D extended structures. The Zn(II) complexes exhibited high emission as compared with their corresponding ligands. Because of their absorbance in the visible region and their green emission, these complexes can be used as candidates for cellular imaging. Thermal study evidenced a decrease in the stability by complexation. Both, ligands and metal complexes were evaluated against bacteria and fungi species and the tests indicated a higher biological activity as compared with the standard compounds Kanamycin and Caspofungin.

Acknowledgments

This research was founded by the Romanian Ministry of National Education under Grant 53/02.09.2013, Cod: PN-II-ID-PCE-2012-4-0261. The authors also acknowledge support by the Austrian–Romanian bilateral mobility grants 749/01.01.2014.

Appendix A. Supplementary data

Supplementary data associated with this article can be found, in the online version, at http://dx.doi.org/10.1016/j.poly.2015.07.030.

References

[1] S.E. Thomas, first ed., Organic Synthesis: The Roles of Boron and Silicon (Oxford Chemistry Primers series), Oxford University Press, 1992. pp. 1–96.
[2] J.B. Lambert, Y. Zhao, R.W. Emblidge, L.A. Salvador, X. Liu, J.-H. So, E.C. Chelius, Acc. Chem. Res. 32 (1999) 183.
[3] W. Noll, Chemistry and technology of silicones, Academic Press, (1968) pp. 210–290.
[4] H. Ito, K. Takagi, T. Miyahara, M. Sawamura, Org. Lett. 7 (2005) 3001.
[5] H. Gotoh, Y. Hayashi, Chem. Commun. (2009) 3083.
[6] P. Nguyen, P. Gomez-Elipe, I. Manners, Chem. Rev. 99 (1999) 1515.
[7] I. Manners, Pure Appl. Chem. 71 (1999) 1471.
[8] Y. Okuda, Y. Ishiguro, S. Mori, K. Nakajima, Y. Nishihara, Organometallics 33 (2014) 1878.
[9] O. Esposito, D.E. Roberts, F.G.N. Cloke, S. Caddick, J.C. Green, N. Hazari, P.B. Hitchcock, Eur. J. Inorg. Chem. 2009 (2009) 1844.
[10] A. Kawachi, Y. Tanaka, K. Tamao, J. Organomet. Chem. 590 (1999) 15.
[11] A.E. Carpenter, G.W. Margulieux, M.D. Millard, C.E. Moore, N. Weidemann, A.L. Rheingold, J.S. Figueroa, Angew. Chem., Int. Ed. 51 (2012) 9412.
[12] P. Braunstein, N.M. Boag, Angew. Chem., Int. Ed. 40 (2001) 2427.
[13] P. Braunstein, M. Knorr, C. Stern, Coord. Chem. Rev. 178–180 (1998) 903.
[14] F. Montilla, V. Rosa, C. Prevett, T. Aviles, M. Nunes da Ponte, D. Masi, C. Mealli, Dalton Trans. (2003) 2170.
[15] M. Cazacu, G. Munteanu, C. Racles, A. Vlad, M. Marcu, J. Organomet. Chem. 691 (2006) 3700.
[16] M. Cazacu, M. Marcu, A. Vlad, M. Vasiliu, J. Macromol. Sci. 5 (2004) 565.
[17] M. Cazacu, M. Marcu, A. Vlad, Gh.I. Rusu, M. Avadanei, J. Organomet. Chem. 689 (2004) 3005.
[18] A. Soroceanu, M. Cazacu, S. Shova, C. Turta, J. Kozisek, M. Gall, M. Breza, P. Rapta, T.C.O. Mac Leod, A.J.L. Pombeiro, J. Telser, A.A. Dobrov, V.B. Arion, Eur. J. Inorg. Chem. (2013) 1458.
[19] M.F. Zaltariov, M. Cazacu, N. Vornicu, S. Shova, C. Racles, M. Balan, C. Turta, Supramol. Chem. 25 (2013) 490.
[20] Y. Cui, X. Dong, Y. Li, Z. Li, W. Chen, Eur. J. Med. Chem. 58 (2012) 323.
[21] P. Gurumoorthy, D. Mahendiran, D. Prabhu, C. Arulvasu, A.K. Rahiman, RSC Adv. 4 (2014) 42855.
[22] A. Bhattacharyya, S. Sen, K. Harms, S. Chattopadhya, Polyhedron 88 (2015) 156.
[23] M.F. Zaltariov, A. Vlad, M. Cazacu, M. Avadanei, N. Vornicu, M. Balan, S. Shova, Spectrochim. Acta 138 (2015) 38.
[24] M.F. Zaltariov, M. Alexandru, M. Cazacu, S. Shova, G. Novitchi, C. Train, A. Dobrov, M.V. Kirillova, E.C.B.A. Alegria, A.J.L. Pombeiro, V.B. Arion, Eur. J. Inorg. Chem. 2014 (2014) 4946.
[25] G.G. Dubinina, H. Furutachi, D.A. Vicic, J. Am. Chem. Soc. 130 (2008) 8600.
[26] M.F. Mahon, J. McGinley, K.C. Molloy, Inorg. Chim. Acta 355 (2003) 368.
[27] P.L. Arnold, S.T. Liddle, J. McMaster, C. Jones, D.P. Mills, J. Am. Chem. Soc. 129 (2007) 5360.
[28] P. Edwards, K. Mertis, G. Wilkinson, M.B. Hursthouse, K.M. Abdul Malik, J. Chem. Soc., Dalton Trans. (1980) 334.
[29] S.-B. Zhao, R.-Y. Wang, S. Wang, Organometallics 28 (2009) 2572.
[30] X. Zhang, B. Cao, E.J. Valente, T.K. Hollis, Organometallics 32 (2013) 752.
[31] A. Soroceanu, M. Cazacu, C. Racles, I. Stoica, L. Sacarescu, C.-D. Varganici, Soft Matter. 13 (2015) 93.
[32] Q.-H. Meng, P. Zhou, F. Song, Y.-B. Wang, G.-L. Liu, H. Li, CrystEngComm 15 (2013) 2786.
[33] CrysAlis RED, Oxford Diffraction Ltd., Version 1.171.36.32, 2003.
[34] O.V. Dolomanov, L.J. Bourhis, R.J. Gildea, J.A.K. Howard, H. Puschmann, J. Appl. Cryst. 42 (2009) 339.
[35] G.M. Sheldrick, SHELXS Acta Cryst. A64 (2008) 112.
[36] S. Zolezzi, A. Decinti, E. Spodine, Polyhedron 18 (1999) 897.
[37] D.M. Adams, Metal Ligand and Related Vibrations, Edward Arnold, London, 1967. pp. 248–284.
[38] K. Nakamoto, In Infrared and Raman Spectra of Inorganic and Coordination Compounds, fouth ed., Wiley-Interscience, New York, NY, 1986. pp.203–236.
[39] J. Gradinaru, A. Forni, Y. Simonov, M. Popovici, S. Zecchin, M. Gdaniec, D.E. Fenton, Inorg. Chim. Acta 357 (2004) 2728.
[40] S.M. Annigeri, A.D. Naik, U.B. Gangadharmath, V.K. Revankar, V.B. Mahale, Transit. Met. Chem. 27 (2002) 316.
[41] Z. Chu, W. Huang, Inorg. Chem. Commun. 11 (2008) 1166.
[42] Z. Chu, W. Huang, L. Wang, S. Gou, Polyhedron 27 (2008) 1079.
[43] A. Bhattacharyya, S. Sen, K. Harms, S. Chattopadhyay, Polyhedron 88 (2015) 156.
[44] S. Basak, S. Sen, S. Banerjee, S. Mitra, G. Rosair, M.T. Garland Rodriguez, Polyhedron 26 (2007) 5104.
[45] M.X. Li, L.Z. Zhang, C.L. Chen, J.Y. Niu, B.S. Ji, J. Inorg. Biochem. 106 (2012) 117.
[46] V.A. Joseph, J.H. Pandya, R.N. Jadeja, J. Mol. Struct. 1081 (2015) 443.
[47] J.R. Anacona, J.L. Rodriguez, J. Camus, Spectrochim. Acta, Part A 129 (2014) 96.